MODELLING OF FLUTTER CHARACTERISTICS OF AIRCRAFT WING WITH PYLON-MOUNTED ENGINE NACELLE

Q. Yu*, S. Lee*, M. Damodaran† and B. C. Khoo†,*
National University of Singapore
***Dept. of Mechanical Engineering, Block EA, 9 Engineering Drive 1, Singapore 117575**
†Temasek Laboratories, T-Lab Building, 5A Engineering Drive 1, Singapore 117411

Keywords: *Wing-Engine-Nacelle Flutter, Continuation Method,*

Abstract

The focus of this work is on applying the Continuation Method (CM) for the aeroelastic analysis of the JAXA Standard Wing Model (JSM) with Pylon-Mounted Engine Nacelle in subsonic and low supersonic flow regimes. The results of standard structural analysis are shown and compared for cases of the JSM with and without engine to formulate a reduced order model for the analysis. The generalized aerodynamic forces (GAF) under different reduced frequencies are calculated using the Doublet Lattice Method (DLM) in the subsonic flow regime and a supersonic lifting surface theory based on the unsteady linearized small disturbance potential flow equation for the low end of the supersonic flow regime. The formulation of the state space form of the system equations based on the Rational Function Approximation (RFA) method and the combination with the continuation method are shown. Flutter analysis results from the continuation method are compared with those from traditional p-k method to elucidate its advantages in efficiency for modes tracking and modes switching phenomenon.

1 Introduction

Flutter is a self-oscillating motion resulting from interactions between aerodynamic forces and structural vibrations which can result in a loss of control or serious damage to the aircraft. For these reasons, flutter characteristics of aircraft structures in fluid flow must be analyzed to mitigate the consequences of flutter during the operation. In this work, the effects of a pylon-mounted engine nacelle on the structural characteristics of the original JAXA Standard Wing Model (*JSM*) which is a wing-body model with high-lift devices and pylon-mounted engine for wind tunnel experiment defined by the Japan aerospace exploration agency (JAXA) and used as a test case for NASA high lift prediction workshop as outlined in [1], are analyzed using the Finite Element Model (FEM). The Continuation Method (CM), as outlined in Meyer [2] combined with the Doublet-Lattice Method (DLM) using the Prandtl-Glauert transformation for compressible subsonic flow as outlined in Albano and Rodden [3] are used to estimate the aerodynamic loads and to analyze the flutter characteristics.

2 Description of Wing-Pylon-Nacelle Model

The main objective of this study is to assess the aeroelastic characteristics of the JSM wing, the properties of which are defined in Yamamoto et al. [4] when a single engine mass is included. For efficient modeling and computation, the original JSM wing is approximated with the finite element model (FEM) using plate elements as shown in Fig. 2.1. The main body of the wing is created with the combination of two sections and the effect of engine mass is simulated as the point mass on the center of gravity inside the engine. The point mass for the engine is located on the center of gravity (CG) of the engine nacelle and

pylon mount which is assumed as 60% of the distance between inlet and the end of the pylon as in Chai et al. [5]. The position of the point mass for the engine implementation, mean aerodynamic chord of the wing and the change in CG location due to the engine mass implementation are shown in Fig. 2.1. As the specifications of the JSM are similar to that of the Boeing B787 series, consequently, the mass of the engine is estimated based on the sample engine, GEnX for B787. The original dry-weight for GEnX is $12822\ lb \approx 5816$ kg and the estimated length ratio between real aircraft and the model is 10:1 which leads to 5.816 kg of point mass applied on the estimated center of gravity for engine nacelle and support. There are 10 grid points on chord-wise direction and 21 points on span-wise direction for the simplified JSM FEM model. The total number of grid points is 210 and the total number of shell elements is 180. The semi-wingspan of the wing model is 2300 mm with a mean aerodynamic chord of 529.2 mm, a leading-edge sweep angle of 33° and a taper ratio of 0.333. The original model is purely for the aerodynamic experiments and the information of the material properties is not known. Hence, the material is assumed to be the as that used in the AGARD 445.6 wing model described in Yates [6]. The moduli of elasticity in the longitudinal direction (E_1) and lateral direction (E_2) are 3.1511 GPa and 0.4162 GPa respectively. The Poisson's ratio (υ) is 0.31, shear modulus (G) is 0.4392 GPa and wing density (ρ) is 381.98 kg/m^3.

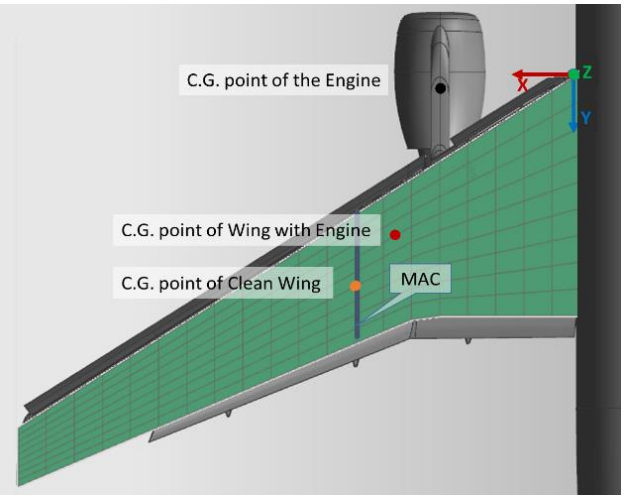

Figure 2.1 Simplified JSM wing model

3 Computational Aeroelastic Modeling

3.1 Modal Analysis and Formulation of Reduced Order System Equations

Considering a three-dimensional simplified wing model with three degrees of freedom, namely plunge ($q_1=h$), pitch ($q_2=\alpha$) and roll ($q_3=\phi$), a modal analysis is carried out in order to establish the reduced-order structural model from the general structural equations defined as

$$\boldsymbol{M\ddot{q} + Cq + Kq = F_{aero}} \qquad (1)$$

where $\boldsymbol{M, C, K}$ are the global mass, damping and stiffness matrices and $\boldsymbol{q}$ is a $n \times 1$ column vector representing the degrees of freedoms for each grid arising from the structural model. The unforced system equations of motion can be expressed as follows in which the aerodynamic forces and moments matrix $\boldsymbol{F_{aero}}$ is set to 0 in Eqn (1). In this study and for the general vibrational modal analysis, the structural damping is also ignored i.e. ($\boldsymbol{C = 0}$). The natural modes and natural frequencies are then computed, and the first 4 natural modes are selected to establish the reduced-order structural model. The generalized mass matrix $\widetilde{\boldsymbol{M}}$, stiffness matrix $\widetilde{\boldsymbol{K}}$, and generalized displacements vector $\widetilde{\boldsymbol{q}}$ are computed as:

$$\begin{aligned} \boldsymbol{\Phi}^{\mathrm{T}}\boldsymbol{M}\boldsymbol{\Phi} &= \widetilde{\boldsymbol{M}} \\ \boldsymbol{\Phi}^{\mathrm{T}}\boldsymbol{K}\boldsymbol{\Phi} &= \widetilde{\boldsymbol{K}} \\ \boldsymbol{\Phi}^{\mathrm{T}}\boldsymbol{q} &= \widetilde{\boldsymbol{q}} \end{aligned} \qquad (2)$$

where $\boldsymbol{\Phi}$ is the modal matrix with the selected structural modes. The first four natural frequencies of the wing with engine together with that of the first two nacelle modes and the clean wing are shown in Table 3.1 and the corresponding mode shapes are shown in Fig. 3.2 and Fig. 3.3 respectively.

Table 3.1: Natural Frequencies of The Clean Wing and Wing with Engine Nacelle Model

#	Mode Frequencies (Nastran)	With Nacelle (Hz)	Clean Wing (Hz)
1	1st bending	1.366	1.1381
2	2nd bending	6.732	6.437
3	1st torsion	12.603	10.768
4	3rd bending	15.356	16.335
5	Nacelle pitching	2.528	-
6	Nacelle rolling	4.446	-

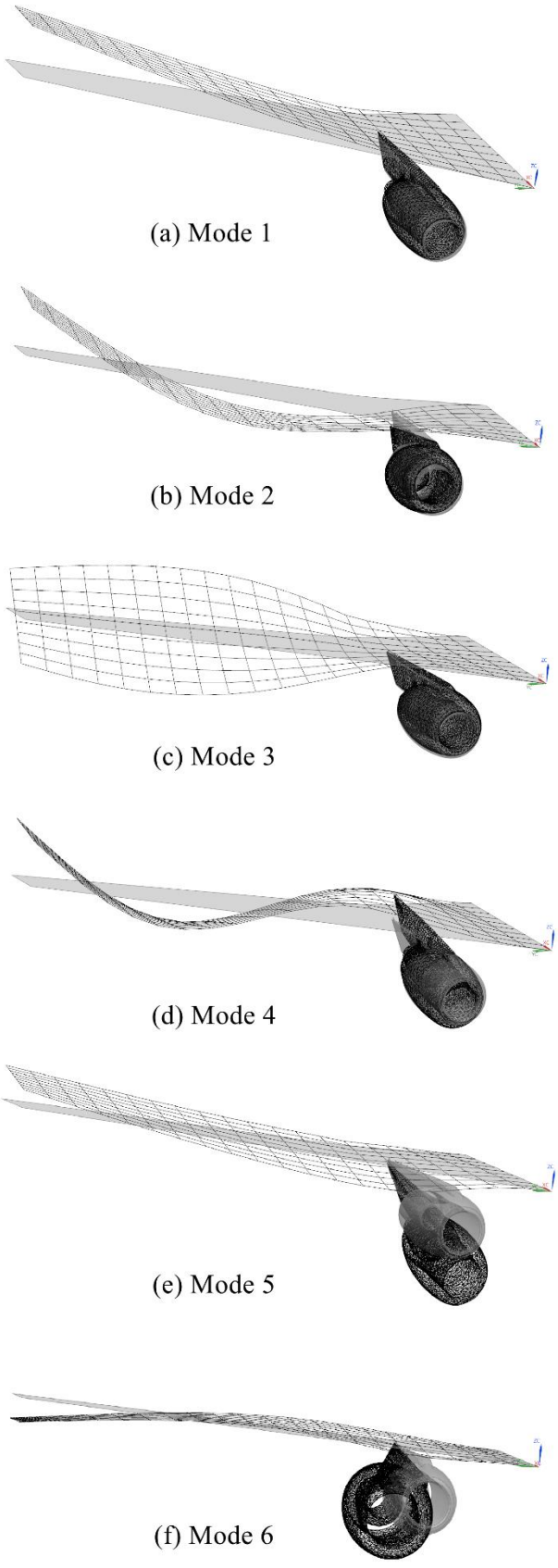

Figure 3.2 The First Six Natural Mode Shapes of the JSM Wing with Engine Nacelle

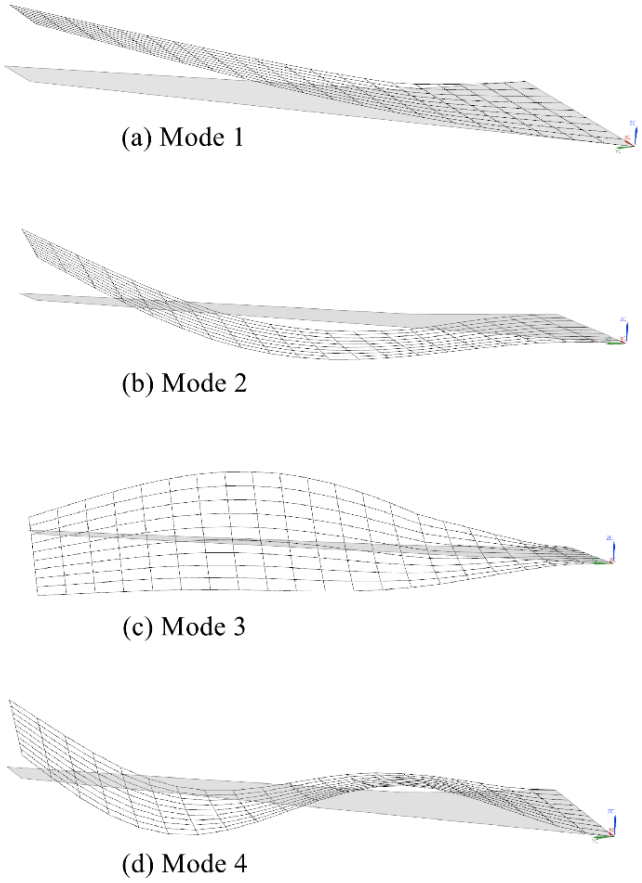

Figure 3.3 The First Four Natural Mode Shapes of the JSM Wing without Engine Nacelle

3.2 Aerodynamic Solvers

Fig. 3.4 shows the aerodynamic model constructed in *Nastran* [7] for the JSM wing model. DLM for subsonic aerodynamic flows and the supersonic lifting surface method outlined in Liu et al. [8] embodied in *ZONA51* [9] for supersonic flows are used to estimate the aerodynamic forces and moments $\boldsymbol{F_{aero}}$ for different reduced frequencies. The linearized unsteady small disturbance potential equation forms the backbone of the aerodynamic model i.e.

$$(1-M_\infty^2)\Phi_{xx}+\Phi_{yy}+\Phi_{zz}-\frac{2M_\infty^2}{U_\infty}\Phi_{xt}-\frac{M_\infty^2}{U_\infty}\Phi_{tt}=0 \quad (3)$$

where Φ is the disturbance velocity potential function, $M_\infty=\frac{U_\infty}{a}$ is the free stream Mach number, U_∞ is the freestream velocity and a is the speed of sound. The differential pressure $\Delta p(x,y,z)$ between the upper surface and lower surface across the wing and the nondimensional

upwash velocity field on the surface of wing i.e. $\overline{w}(x,y,z)$ are related via a kernel function based on the assumption of small deflection harmonic motion outlined in Albano and Rodden [3] as :

$$\overline{w}(x,y,z) = -\frac{1}{4U_\infty \pi \rho} \iint \Delta p(x,y,z)\, K(x-\xi, y-\eta, z) d\xi d\eta \qquad (4)$$

where ρ is the density of the fluid, ξ and η are dummy variables of integration over the wing surface, K is the approximated kernel function along the 1/4 chord line of each box element. In subsonic flow region, the unknown lifting pressures are assumed to be concentrated uniformly across the one-quarter chord line of each box. There is one control point per box, centered spanwise at the three-quarter chord line of the box, and the surface boundary condition of no normal flow is satisfied at each of these points. The solutions of Eqn (4) give the relation between the pressure coefficient differences $\Delta\tilde{C}_p$and the upwash velocity field as:

$$\{\Delta\widetilde{\boldsymbol{C}}_{\boldsymbol{p}}\} = [\boldsymbol{A.I.C}\ (M_\infty, k)]\{\overline{\boldsymbol{w}}\} \qquad (5)$$

where $[\boldsymbol{A.I.C}\ (M_\infty, k)]$ is aerodynamic influence coefficient matrix which is a function of Mach number and reduced frequency *k* which is regarded as a key parameter in aeroelastic analysis that relates the structural motions to the aerodynamic forces. The 180 aerodynamic boxes are tied to the 210 grid points which are uniformly spaced spanwise from the root to tip of the wing. The density of air is assumed to be 1.225 kg/m^3 and the Mach number for subsonic and supersonic region is varied in the range 0.1~0.8 and 1.1~1.4, respectively. The range of airspeed is varied from 4.8 m/s to 210 m/s to find the instabilities for each Mach number. Considering the generalized aerodynamic forces arising from the aerodynamic models for subsonic and low speed supersonic regions, the reduced-order governing equations for the JSM wing can be written as follows:

$$\widetilde{\boldsymbol{M}}\ddot{\widetilde{\boldsymbol{q}}} + \widetilde{\boldsymbol{K}}\widetilde{\boldsymbol{q}} = q_\infty \boldsymbol{A.I.C}(M_\infty, k)\widetilde{\boldsymbol{q}} \qquad (6)$$

where $q_\infty = \frac{1}{2}\rho U_\infty^2$ is a dynamic pressure.

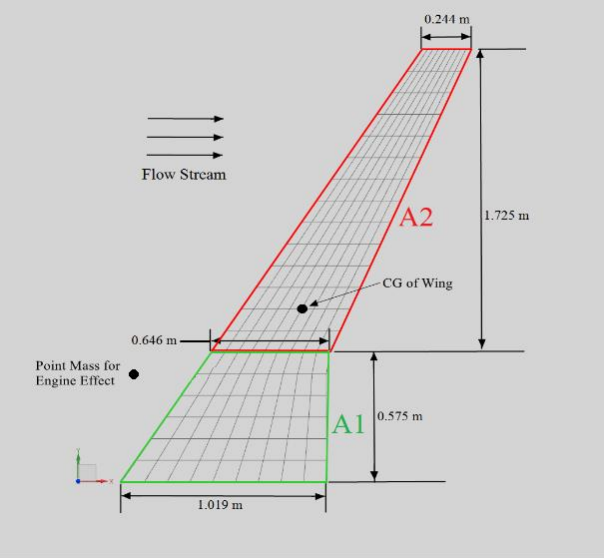

Figure 1.4 Aerodynamic Model for JSM Wing with Engine Mass based on DLM Method

3.3 Introduction of the Continuation Method

The Continuation Method (CM) can be described as "a continuous transformation from one function to another" as in Weisstein [10]. It was originally introduced to solve the algebraic nonlinear problems in which the solution is treated as an instant of a dynamic problem as in Ogrodzki [11]. In the Continuation Method, an auxiliary equation is chosen properly and constructed to solve the original problem. For example, if the original problem is $\boldsymbol{f}(\boldsymbol{x}) = 0$, then one example of the CM equation can be written as follows:

$$\boldsymbol{H}(\boldsymbol{x}, \lambda) = \lambda \boldsymbol{f}(\boldsymbol{x}) + (1-\lambda)\boldsymbol{g}(\boldsymbol{x}) = \boldsymbol{0} \qquad (7)$$

The idea of the continuation method is that an easy function is chosen as $\boldsymbol{g}(\boldsymbol{x})$ and the parameter λ is swept from 0 to 1, so that the easy problem is continuously deformed into the original problem as outlined in Vesa Linja – aho [12] which is the approach used in this work. The parameter λ could also be chosen as one of the system variables. The continuation function $\boldsymbol{H}(\boldsymbol{x}, \lambda)$ may be constructed and solved in numerous ways. The concept of using a continuation method for solving a set of nonlinear equations consists of the formation of the CM function, choosing an efficient solver and making a working implementation of these. Generally, the continuation methods are much less sensitive to the initial guess than the

Newton–Raphson method. Some continuation methods can be globally convergent with certain conditions as in Vesa Linja – aho [12]. Common to all the continuation methods, there is a predictor phase followed by a corrector phase as shown in Fig.3.5. Starting from a known solution, the predictor phase computes a starting guess which is then used by the corrector to obtain the true solution at the new value of the continuation parameter as shown in Meyer [2]. The tangent vector **t** is often used as the predictor in the continuation method to determine the direction of the predictor for each step shown in Figure 3.5. It can be defined as $\mathbf{Jt} = \mathbf{0}$ where $\mathbf{J} = \partial \mathbf{H} / \partial(\mathrm{x}, \lambda)$ is the Jacobian matrix of the original nonlinear equations. Noting that the Jacobian matrix **J** is a $\mathrm{n} * (\mathrm{n}+1)$ non-square matrix and the tangent vector $\mathbf{t} = [\mathrm{x}_1\ \mathrm{x}_2 \ldots \mathrm{x}_\mathrm{n}\ \lambda]^\mathrm{T}$ is a $(\mathrm{n}+1)$ dimensional column vector implying that $\mathbf{Jt} = \mathbf{0}$ contains n equations with (n+1) unknowns. Hence a normalization condition is necessary to obtain the unique tangent vector in each iteration step by choosing the condition: $\mathbf{t}^\mathrm{T}\mathbf{t} = 1$. Newton-Raphson's method is usually chosen to be the corrector algorithm since it has proven to be very efficient in solving the nonlinear equations when a good initial guess from the predictor is given:

$$\{\boldsymbol{x_{i+1}}\} = \{\boldsymbol{x_i}\} - [\boldsymbol{J}]^{-1}\boldsymbol{f}(\boldsymbol{x}) \qquad (8)$$

Another important point is that during the corrector phase followed by the next predictor phase, the continuation parameter λ is fixed to avoid singularities in algorithm. For example, after the prediction point $(\hat{\mathbf{x}}_\mathrm{N}, \lambda_\mathrm{N})$ in Fig. 3.5 has been computed based on the previous accurate point $(\mathbf{x}_{\mathrm{N}-1}, \lambda_{\mathrm{N}-1})$ and tangent vector $\mathbf{t}_{\mathrm{N}-1}$, then λ should be fixed at $\lambda = \lambda_N$ in the following corrector phase in order to let the correction algorithm work properly to get the accurate point $(\mathbf{x}_\mathrm{N}, \lambda_\mathrm{N})$ in the path.

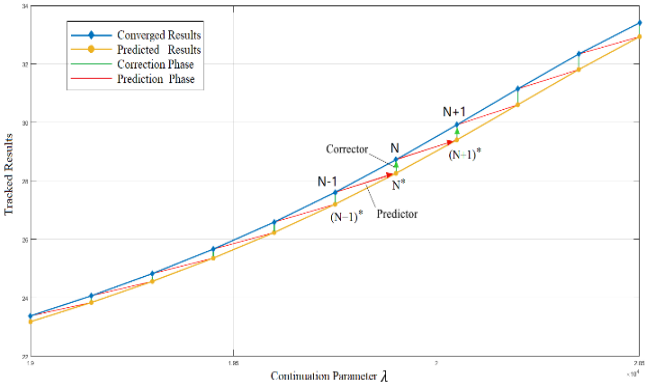

Figure 3.5. Path tracking based on Continuation Method

3.4 Application of Continuation Method in Flutter Analysis

Recalling the reduced order system equation for the JSM wing model as

$$\widetilde{\boldsymbol{M}}\ddot{\widetilde{\boldsymbol{q}}} + \widetilde{\boldsymbol{K}}\widetilde{\boldsymbol{q}} = q_\infty \boldsymbol{A.I.C}(M_\infty, k)\widetilde{\boldsymbol{q}} \qquad (9)$$

for a fixed Mach number and a series of reduced frequencies ranging from 0.0 to 1.5 is chosen to compute the $\boldsymbol{A.I.C}(M_\infty, k)$ matrices from the aerodynamic solver, noting that the original $\boldsymbol{A.I.C}(M_\infty, k)$ can only be listed for a series of discrete reduced frequencies for a fixed Mach number M_∞. Hence the Rational Function Approximation (RFA) method is then applied to convert the $\boldsymbol{A.I.C}(M_\infty, k)$ from frequency domain to the Laplace domain in the form of classic Roger's formula shown in *ZAERO* Reference Manual [9], i.e.:

$$\widehat{[\boldsymbol{A.I.C}(p)]} = [\boldsymbol{A_0}] + [\boldsymbol{A_1}]p + [\boldsymbol{A_2}]p^2 + \sum_{l=3}^{n_l+2}[\boldsymbol{A_l}]\frac{p}{p+\gamma_{l-2}} \qquad (10)$$

where p is the non-dimensional Laplace variable $p = sb/V$, n_l is the number of lag terms. ($n_l = 3$ in our case), γ_i is the root value of each lag term which can be chosen by the following empirical formula from *ZAERO* Reference Manual [9].

$$\gamma_i = 1.7 k_{max}\left(\frac{i}{n_l+1}\right)^2 \qquad (11)$$

When converting the $\boldsymbol{A.I.C}(M_\infty, k)$ matrices from frequency domain to Laplace domain, either of the formulations based on Least Squares (LS), Modified Matrix Pade (MMS) or Minimum State (MS) is used for the curve fitting as outlined

in Tiffany and Adams [13]. Part of the results are shown in Fig. 3.6.

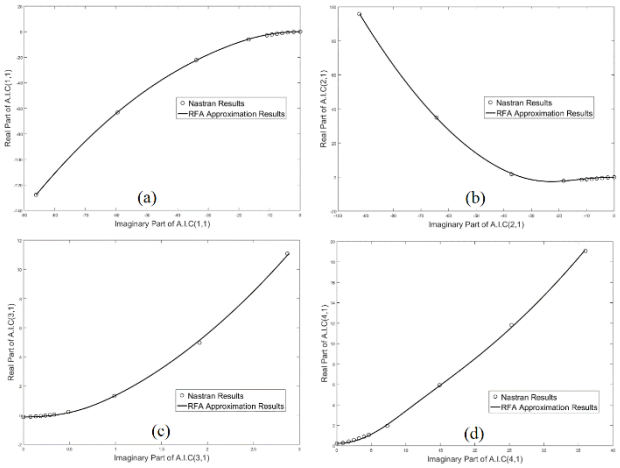

Figure 3.6. Approximation Results of $\boldsymbol{A.I.C}(Ma,k)$ based on RFA method

The reduced order system equations are then transformed to:

$$\widetilde{\boldsymbol{M}}\ddot{\boldsymbol{q}} + \widetilde{\boldsymbol{D}}\dot{\boldsymbol{q}} + \widetilde{\boldsymbol{K}}\boldsymbol{q} - q_{dyn}\boldsymbol{A_3}Y_1 - q_{dyn}\boldsymbol{A_4}Y_2 - q_{dyn}\boldsymbol{A_5}Y_3 = 0 \quad (12)$$

where the lag term variable $\boldsymbol{Y_i} = \frac{\bar{s}}{\bar{s}+\gamma_i}\widetilde{\boldsymbol{q}}$, the modified $\bar{s} = jk$, $\widetilde{\boldsymbol{M}} = \overline{\boldsymbol{M}} - q_{dyn}\boldsymbol{A_2}\left(\frac{b}{V}\right)^2$, $\widetilde{\boldsymbol{D}} = \overline{\boldsymbol{D}} - q_{dyn}\boldsymbol{A_1}\left(\frac{b}{V}\right)^2$ and $\widetilde{\boldsymbol{K}} = \overline{\boldsymbol{K}} - q_{dyn}\boldsymbol{A_0}$. Hence the state space form system equations can be set up as:

$$\dot{\boldsymbol{X}} = \boldsymbol{A}\boldsymbol{X} \quad (13)$$

where $\boldsymbol{X} = \left[\dot{\widetilde{\boldsymbol{q}}}\ \ddot{\widetilde{\boldsymbol{q}}}\ \dot{Y}_1\ \dot{Y}_2\ \dot{Y}_3\right]$ and the matrix $\boldsymbol{A}$ is

$$\begin{pmatrix} 0 & I & 0 & 0 & 0 \\ -\widetilde{\boldsymbol{M}}^{-1}\widetilde{\boldsymbol{K}} & -\widetilde{\boldsymbol{M}}^{-1}\widetilde{\boldsymbol{D}} & q_{dyn}\widetilde{\boldsymbol{M}}^{-1}\boldsymbol{A_3} & q_{dyn}\widetilde{\boldsymbol{M}}^{-1}\boldsymbol{A_4} & q_{dyn}\widetilde{\boldsymbol{M}}^{-1}\boldsymbol{A_5} \\ 0 & \boldsymbol{I} & -(V\gamma_1\,\boldsymbol{I})/b & 0 & 0 \\ 0 & \boldsymbol{I} & 0 & -(V\gamma_2\,\boldsymbol{I})/b & 0 \\ 0 & \boldsymbol{I} & 0 & 0 & -(V\gamma_3\,\boldsymbol{I})/b \end{pmatrix}$$

The main drawbacks of the RFA method is the trade-off between the number of aerodynamic lags and the accuracy of the approximation as pointed out in Edwards [14]. For the analysis of the complex wing models in the continuation method, the approximation errors for $\widetilde{\boldsymbol{A.I.C}}(s)$ using RFA Method cannot be ignored. In this situation, another approach is to calculate $\boldsymbol{A.I.C}(M_\infty, k)$ using cubic spline method under different reduced frequencies followed by the update of the system equations simultaneously in each iteration. Figure 3.7 shows the flow chart of each iteration when combining continuation method with cubic spline method for modes tracking in the flutter analysis.

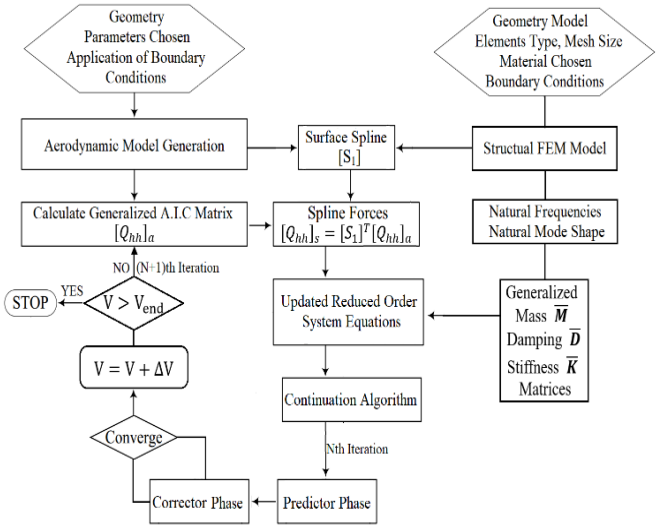

Figure 3.7. Flow Chart of Applying Continuation Method in Modes Tracking for Flutter Analysis

4 Results, Analysis and Discussions

4.1 Modes tracking results in flutter analysis

The first four selected natural modes are tracked using both the traditional p-k method outlined in Hassig [15] and the continuation method based on 1st order state space system equations or the original 2nd order system equations to find the flutter speed corresponding to different flow Mach numbers. In the p-k method for classical flutter computations, the solutions can be expressed in the following form:

$$\widetilde{\boldsymbol{q}} = \overline{\boldsymbol{q}}e^{pt} \quad (14)$$

where $\overline{\boldsymbol{q}}$ is the complex eigenvector, $p = \sigma + i\omega$, σ is the damping which indicates the instability when $\sigma > 0$ while ω represents the angular frequencies. Substituting this into the original reduced order system equations (9) results in:

$$\left[p^2\widetilde{\boldsymbol{M}} + \widetilde{\boldsymbol{K}} - q_\infty \boldsymbol{A.I.C}(M_\infty, k)\right]\overline{\boldsymbol{q}} = \boldsymbol{0} \quad (15)$$

By solving the above second order equations iteratively, we can get a series of isolated point solutions for different airspeeds U_∞ and damping σ. The corresponding results are shown in Figures 4.1 to 4.7. In Fig 4.1 corresponding to

JSM wing without engine, mode 1 is the flutter mode since it reaches flutter (as the damping goes to zero) at 119.8 m/s before Mode 2 which is stable until 140.6 m/s under fixed Mach=0.1 in Fig. 4.1 and Fig.4.2.

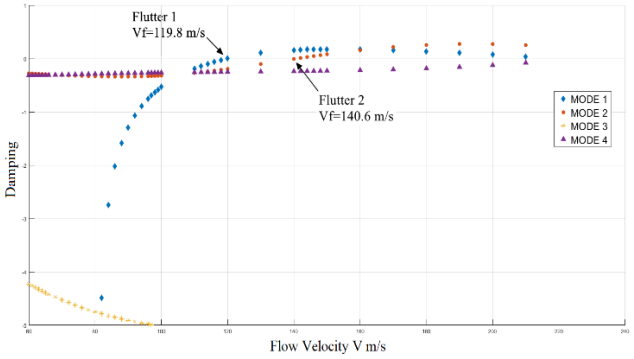

Figure 4.1 Modes Tracking for JSM Wing without Engine using p-k method

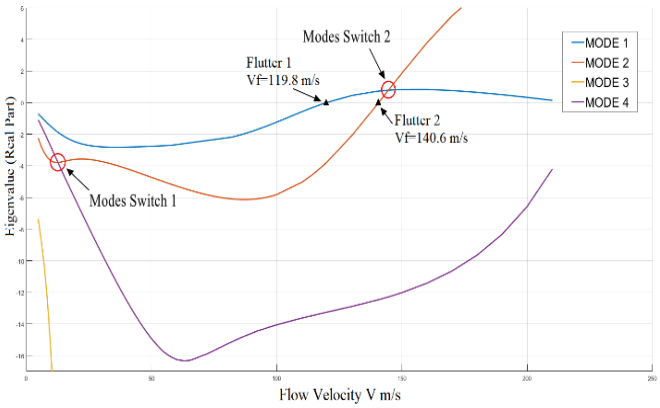

Figure 4.2. Modes Tracking for JSM Wing without Engine using Continuation Method

However, for the case of the JSM wing with engine, which results in significant changes to the mass and stiffness matrices, it can be seen from Figs. 4.3-4.4 that Mode 2 becomes the flutter mode since it reaches flutter at 91.3 m/s

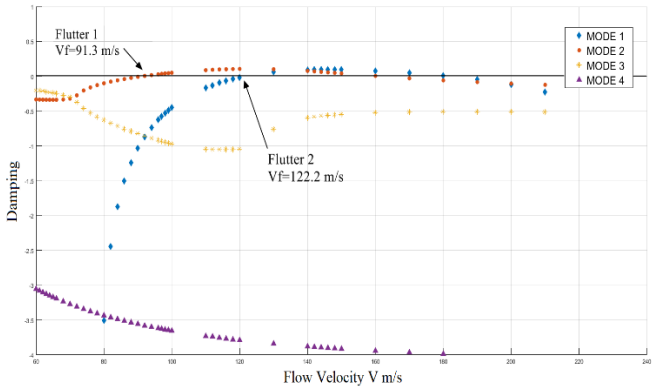

Figure 4.3. Modes Tracking for JSM Wing with Engine using p-k method

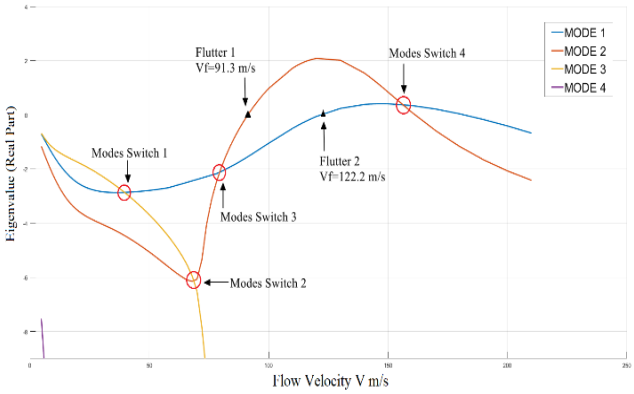

Figure 4.4. Modes Tracking for JSM Wing with Engine using Continuation Method

earlier than Mode 1 which reaches flutter at 122.2 m/s.

The inclusion of the engine nacelle decreases the flutter speed by around 28 m/s. The continuation method enables the tracking of the frequency components of each mode as shown in Fig. 4.5 and Fig. 4.6. As the velocity reaches the flutter point, the two associated frequencies get closer to each other. This phenomenon known as 'frequency coalescence' implies that the energy transfer between the two modes which is usually considered as one of the reasons for flutter occurrence. Fig. 4.7 shows the change of flutter speed in subsonic region and low speed supersonic region as Mach number increases from 0.1 to 1.3.

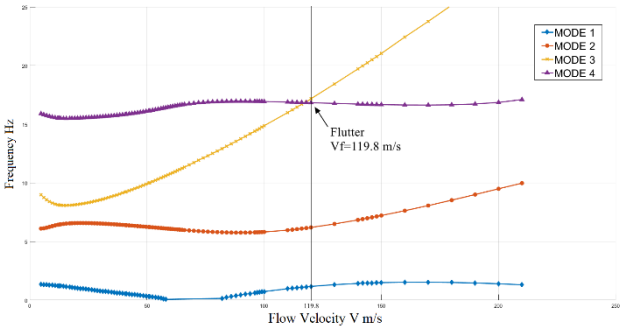

Figure 4.5. Frequency Tracking for JSM Wing without Engine

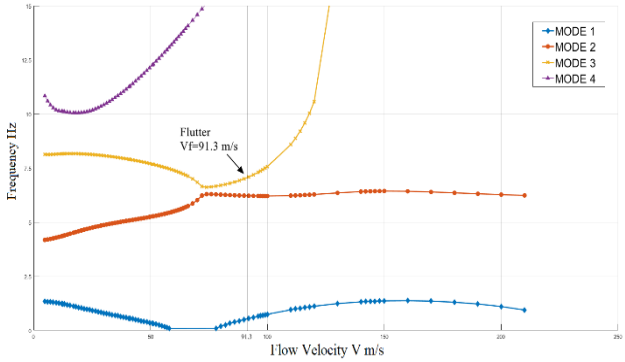

Figure 4.6. Frequency Tracking for JSM Wing with Engine

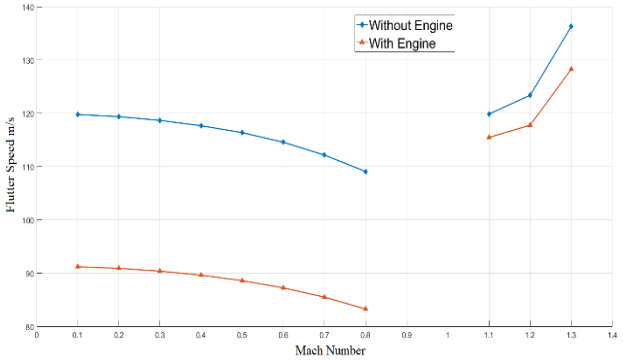

Figure 4.7. Flutter Speed of JSM Wing without Engine under varying Mach Number

4.2 Discussion about Modes Switching Phenomenon

Modes switching phenomenon is widely observed in the modes tracking task and it is defined as when the parameters of interest change, which usually is the airspeed, several different modes will get closer to each other and finally cross at some points. However, using traditional methods like eigenvalue analysis or p-k method may sometimes cause difficulties in recognizing each mode from the crossing point and even lead to potential errors for flutter analysis. As an example, Fig. 4.8 shows the results of the first 6 modes tracking using p-k method for the JSM wing without engine under Mach number 1.2, when airspeed reaches to 45 m/s, three mode shape curves almost cross at one point. Under this situation, a natural way to fix this phenomenon is to connect the points manually, but this is not efficient and in some situations, it is difficult to tell the different modes apart if too many selected modes all cross near one point. However, this issue in modes tracking task is well handled using continuation method which seldom fails in recognizing the modes switching phenomenon. This is because in the prediction phase it can predict the right direction of each mode curve based on the previously corrected points. A smaller step size will be automatically chosen in the algorithm when it detects the modes curve steepen and folds to be multiple-valued. This is realized by monitoring both the curve slope and the number of iterations in corrector phase because the greater the number of iterations usually implies the occurrence of a steeper curve or fold back phenomenon. The fixed curve in modes tracking and frequency tracking by using continuation method are shown in Figs. 4.9 and 4.10.

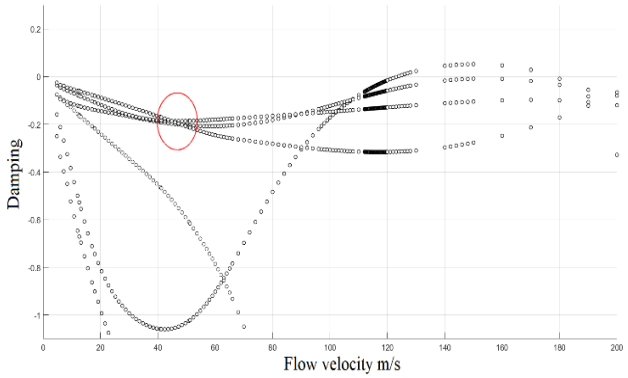

Figure 4.8. Original Result Points for JSM Wing without Engine using p-k method under Mach=1.2

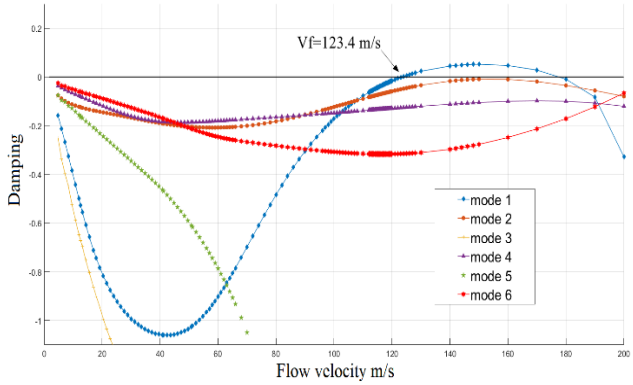

Figure 4.9. Modes Tracking for JSM Wing without Engine using Continuation Method under Mach=1.2

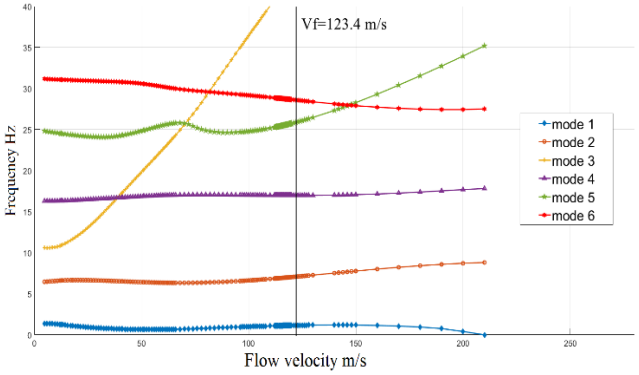

Figure 4.10. Frequency Tracking for JSM Wing without Engine using Continuation Method under Mach=1.2

5 Conclusion

In this work, the flutter analysis of a JSM Wing with a pylon-mounted engine nacelle is considered with the finite element model (FEM) based on *Nastran*. The corresponding results of standard structural analysis are shown and compared for both JSM Wing with and without engine mass to construct the reduced order model. The generalized aerodynamic forces under different reduced frequencies are calculated using Doublet Lattice Method for subsonic regime and ZONA 51 method for the lower end of the supersonic flow regime. Both of these linearized panel methods are based on a series of assumptions such as infinitesimal deflections, inviscid flow and flat plate wing model which will bring some potential inaccuracies. In addition, for the current work, the follower force caused by the engine thrust has been ignored during the flutter analysis. This effect can be taken into consideration by conducting a static aeroelastic analysis before the flutter analysis in the future work. To extend the application of Continuation Method into 3D aircraft wing flutter analysis, two different methods 1) Rational Function Approximation (RFA) 2) Cubic Spline are discussed detailedly. The results of flutter prediction and frequencies tracking based on Continuation Method for both JSM wing with and without engine implementation are obtained in subsonic region (M_∞=0~0.8) and low speed supersonic region (M_∞=1.1~1.4). For the transonic region, the combination between the calculation of generalized aerodynamic forces based on CFD simulation and the continuation method is necessary and will be shown in the future work. Traditional p-k method has also been applied for the flutter analysis. The corresponding results of modes tracking and frequencies tracking are compared with continuation method which show the advantages of efficiency in modes tracking and fixing the errors in modes switching phenomenon.

References

[1] The NASA high lift prediction workshop https://hiliftpw.larc.nasa.gov/ associated with *AIAA Applied Aerodynamics Technical Committee* at the annual *AIAA Aviation Forum and Aerospace Exposition*. (From 2010 onwards)

[2] Meyer E. E., "Application of a New Continuation Method to Flutter Equation," *29th AIAA Structures, Structural Dynamics and Materials Conference*, Williamsburg, Virginia, USA, 18-20 April 1988; doi:10.2514/6.1988-2350

[3] Albano, E., and Rodden, W. P., "A Doublet-Lattice Method for Calculating Lift Distributions on Oscillating Surfaces in Subsonic Flows," *AIAA Journal*, Vol. 7, No.2, pp. 279-285, 1969.

[4] Yokokawa, Y., Murayama, M., Uchida, H., Tanaka, K., Ito, T., Yamamoto, K., and Yamamoto, K., Aerodynamic Influence of a Half-Span Model Installation for High-Lift Configuration Experiment., *48th AIAA Aerospace Sciences Meeting including the New Horizons Forum and Aerospace Exposition*, Orlando, 2010.

[5] Chai, S., Crisafulli, P., and W.H. Mason, "Aircraft Center of Gravity Estimation in Conceptual/Preliminary Design," AIAA 95-3882 in Proceedings of the *1st AIAA Aircraft Engineering, Technology, and Operations Congress* , Los Angeles, CA, 1995

[6] Yates, E. C. (1987) "AGARD Standard Aeroelastic Configurations for Dynamic Response: Candidate configuration I-wing 445.6", NASA-TM-100492, NASA Langley Research Center, Hampton, VA, USA.

[7] Reymond, M. (1994). MSC/NASTRAN quick reference guide: Version 68. Los Angeles/Calif.: MacNeal-Schwendler.

[8] Liu, D., Chen, P. C., Pototzky, A. S., & James, D. K. (1991). Further studies of harmonic gradient method for supersonic aeroelastic applications. Journal of Aircraft, 28(9), 598-605. doi:10.2514/3.46070

[9] ZAERO Version 9.2, (2016), Theoretical Manual, ZONA Technology, Inc; Scottsdale, Arizona, USA; www.zonatech.com

[10] E. W. Weisstein, CRC Concise Encyclopedia of Mathematics, CRC Press,1999.

[11] Ogrodzki, J. (1994), “Circuit Simulation Methods and Algorithms,” CRC Press, Boca Raton, Florida, USA ISBN 9780849378942

[12] Vesa Linja – aho. (2016) “Homotopy Methods in DC Circuit Analysis”, Master of Science in Technology Thesis, Helsinki University of Science and Technology, Helsinki, Finland.

[13] Tiffany, S., & Adams, J. W. (1987). “Nonlinear Programming Extensions to Rational Function Approximations of Unsteady Aerodynamics,” *28th AIAA Structures, Structural Dynamics and Materials Conference*, Monterey, California, USA 6-8 April 1987; doi:10.2514/6.1987-854

[14] John W. Edwards. "Unsteady Aerodynamic Modeling for Arbitrary Motions", *AIAA Journal*, Vol. 15, No. 4 (1977), pp. 593-595.

[15] Hassig, H. J., “An Approximate True Damping Solution of the Flutter Equation by Determinant Iteration,” *AIAA Journal of Aircraft*, Vol. 8, No. 11, 1971, pp. 885–889. doi:10.2514/3.44311

Copyright Statement